HHS Public Access

Author manuscript

Int J Cancer. Author manuscript; available in PMC 2020 April 01.

Published in final edited form as:

Int J Cancer. 2019 December 01; 145(11): 2986–2995. doi:10.1002/ijc.32334.

SET domain containing 1B gene is mutated in primary hepatic neuroendocrine tumors

Penghui Yang[1,2,*], **Xuanlin Huang**[3,*], **Chengcai Lai**[2,*], **Lin Li**[3,4,*], **Tieling Li**[5], **Peide Huang**[3,6], **Songying Ouyang**[7,8], **Jin Yan**[1], **Sijie Cheng**[1], **Guanglin Lei**[1], **Zhaohai Wang**[1], **Linxiang Yu**[1], **Zhixian Hong**[1], **Ruisheng Li**[1], **Hui Dong**[9], **Cheng Wang**[5,10], **Yinghao Yu**[11], **Xuan Wang**[12], **Xianghong Li**[13], **Liming Wang**[14], **Fudong Lv**[15], **Ye Yin**[3], **Huanming Yang**[3,16], **Jianxun Song**[17], **Qiang Gao**[3,†], **Xiliang Wang**[2,†], **Shaogeng Zhang**[1,†]

[1]Beijing 302 Hospital/5th Medical Center of Chinese PLA General of Hospital, Beijing, China

[2]State Key Laboratory of Pathogens and Biosecurity, Beijing Institute of Microbiology and Epidemiology, Beijing, China

[3]BGI-Shenzhen, Shenzhen, China

[4]Shanghai Clinical Center for Endocrine and Metabolic Diseases, Shanghai Key Laboratory for Endocrine Tumors, Rui-Jin Hospital, Shanghai Jiao-Tong University School of Medicine, Shanghai, China

[5]Chinese PLA General Hospital, Beijing, China

[6]Section of Molecular Disease Biology, Department of Veterinary Disease Biology, Faculty of Health and Medical Sciences, University of Copenhagen, Copenhagen, Denmark

[7]The Key Laboratory of Innate Immune Biology of Fujian Province, Biomedical Research Center of South China, Key Laboratory of OptoElectronic Science and Technology for Medicine of Ministry of Education, College of Life Sciences, Fujian Normal University, Fuzhou, China

[8]Provincial University Key Laboratory of Cellular Stress Response and Metabolic Regulation, College of Life Sciences, Fujian Normal University, Fuzhou, China

[9]Eastern Hepatobiliary Surgery Institute/Hospital, Shanghai, China

[10]Beijing 307 Hospital Affiliated with the Academy of Medical Sciences, Beijing, China

[11]Fuzhou General Hospital of Nanjing Military Command of Chinese PLA, Fuzhou, China

[12]The 81st Hospital of PLA, Nanjing, China

[13]Key Laboratory of Carcinogenesis and Translational Research (Ministry of Education), Peking University Cancer Hospital & Institute, Beijing, China

Correspondence to: Qiang Gao, BGI-Shenzhen, Shenzhen 518083, China, gaoqiang@genomics.cn; or Xiliang Wang, State Key Laboratory of Pathogens and Biosecurity, Beijing Institute of Microbiology and Epidemiology, Beijing 100071, China, xiliangw@126.com; or Shaogeng Zhang, Beijing 302 Hospital/5th Medical Center of Chinese PLA General of Hospital, Beijing 100039, China, zhangsg302@hotmail.com.

*P.Y., X.H., C.L. and L.L. contributed equally to this work

†These authors jointly directed this work

Conflict of interest: None declared.

Additional Supporting Information may be found in the online version of this article.

[14]Cancer Hospital Chinese Academy of Medical Science, Beijing, China

[15]Beijing You'an Hospital, Capital Medical University, Beijing, China

[16]James D. Watson Institute of Genome Sciences, Hangzhou, China

[17]Microbial pathogenesis and Immunology, Texas A&M University College of Medicine, Bryan, TX

Abstract

Primary hepatic neuroendocrine tumors (PHNETs) are extremely rare NETs originating from the liver. These tumors are associated with heterogeneous prognosis, and few treatment targets for PHNETs have been identified. Because the major genetic alterations in PHNET are still largely unknown, we performed whole-exome sequencing of 22 paired tissues from PHNET patients and identified 22 recurring mutations of somatic genes involved in the following activities: epigenetic modification (*BPTF*, *MECP2* and *WDR5*), cell cycle (*TP53*, *ATM*, *MED12*, *DIDO1* and *ATAD5*) and neural development (*UBR4*, *MEN1*, *GLUL* and *GIGYF2*). Here, we show that *TP53* and the SET domain containing the 1B gene (*SETD1B*) are the most frequently mutated genes in this set of samples (3/22 subjects, 13.6%). A biological analysis suggests that one of the three *SETD1B* mutants, A1054del, promotes cell proliferation, migration and invasion compared to wild-type *SETD1B*. Our work unveils that *SETD1B* A1054del mutant is functional in PHNET and implicates genes including *TP53* in the disease. Our findings thus characterize the mutational landscapes of PHNET and implicate novel gene mutations linked to PHNET pathogenesis and potential therapeutic targets.

Keywords

PHNETs; whole-exome sequencing; *SETD1B*

Introduction

Neuroendocrine tumors (NETs) have an average annual incidence of 2 per 100,000 cases among all tumors of the gastrointestinal (GI) tract. NETs are derived from neuroendocrine cells that are capable of producing functional peptide hormones. Typically, these tumors are found in the GI tract (55%) and lungs (30%), although they can also arise in the pancreas (2%), reproductive system (1%), biliary tract (1%) and head and neck (0.4%), among other areas.[1] GI NETs frequently metastasize to the liver, but primary NETs of hepatic origin are extremely rare.[2] According to the 2010 World Health Organization (WHO) classification system, primary hepatic neuroendocrine tumors (PHNETs) are divided into three grades (1–3) based on their histological criteria. Ultrasound, CT and MRI are all typically employed to characterize these lesions, but their appearance on diagnostic imaging can be highly variable and often mimics the features of more common hepatic malignancies. Due to the rarity of PHNETs, their clinical features and treatment outcomes are largely unknown, but there remains a compelling need to extensively identify genomic abnormalities underlying PHNETs and to elucidate their molecular basis for the purpose of guiding effective clinical therapies.

Here, we present the mutational landscape of PHNETs using whole-exome sequencing (WES) to identify tumor recurrent mutations in multiple genes involving disrupted pathways. We report for the first time the identification of somatic mutations in the SET domain containing 1B gene (*SETD1B*) in PHNETs. One of the three *SETD1B* mutants, A1054del, confers a more aggressive PHNET phenotype. This is the largest genomic sequencing study of PHNETs and represents major progress toward the complete molecular characterization of this rare tumor, which may help improve its clinical management.

Materials and Methods

Clinical sample collection

PHNET tissue samples from the livers of confirmed PHNET patients were collected from Beijing 302 Hospital, Eastern Hepatobiliary Surgery Institute/Hospital, Chinese PLA General Hospital, Beijing 307 Hospital, Fuzhou General Hospital of Nanjing Military Command of Chinese PLA, Peking University Cancer Hospital & Institute, Cancer Hospital Chinese Academy of Medical Science and Beijing You'an Hospital. All patients included in our study were clinically diagnosed with PHNETs, and all tumors were confirmed based on pathology, MRI, CT or PET-CT. All of the samples used in our study were residual specimens collected after diagnosis, and none of the patients received treatment prior to sample collection. Matched normal tissues were collected from adjacent liver tissue 5 cm from the border of the surgical area. Informed consent was obtained from all study participants. All experimental protocols were approved by the Beijing 302 Hospital Ethics Committee.

All tumor and normal samples were subjected to hematoxylin staining and histopathological review to assess the presence of tumor cells, normal liver cells, lymphocytic infiltration and necrotic cells. Tumor cellularity was visually scored in a semiquantitative fashion and only tumors with >80% of malignant cells were used for sequencing. The tumor histology was centrally reviewed and validated according to the WHO guidelines. WES of the paired tumor and nonadjacent normal tissue samples from 22 patients were performed. Mass spectrometric genotyping was used to ensure that the tumor DNA and normal DNA were derived from the same patient.

DNA sample preparation

Frozen and formalin-fixed paraffin-embedded (FFPE) tumor tissue samples with matched adjacent tissues from 22 PHNET patients were obtained for WES. Genomic DNA was extracted from frozen samples with a DNeasy Blood and Tissue Mini Kit (Qiagen, Hilden, Germany), and genomic DNA was extracted from FFPE samples with a QIAamp DNA FFPE Tissue Kit (Qiagen) according to the manufacturer's instructions. Sample testing included the sample concentration, integrity and purity. The sample concentration was detected by a fluorometer or Microplate Reader (Qubit Fluorometer, Invitrogen, Carlsbad, CA). Sample integrity and purity were detected by Agarose Gel Electrophoresis (concentration of agarose gel: 1%, voltage: 150 V, and electrophoresis time: 40 min).

Exome capture and sequencing

The qualified genomic DNA from 22 PHNET patients was fragmented by Covaris Technology (Woburn, MA) into library fragments that were 200–300 bp in size, and adapters were ligated to both ends of the fragments. The extracted DNA was amplified, purified and hybridized to the Nimble GenSeqCap EZ Exome 64M (V3) human exome array for enrichment. Both noncaptured and captured PCR products were subjected to real-time PCR to estimate the degree of enrichment. Each captured library was loaded on a HiSeq4000 platform. The raw data were processed using the base-calling module (version 1.7) for base calling, and the sequences of the samples from each individual were generated as 90-bp paired-end reads.

Reads mapping and variation calling

Sequence tags were mapped to the hg19 human genome reference sequence using the Burrows–Wheeler Aligner (BWA, version: 0.5.9-r16). Somatic point mutations were detected by VarScan2.2.5 using the following parameters: SAM tools (v0.1.18) mpileup −Q 0 && VarScan2.2.5 somatic –min-coverage10 –min-coverage-normal 10 –min-coverage-tumor 10 –min-var-freq 0.1 –min-avg-qual 0. Somatic indels were predicted with the GATK Somatic Indel Detector using default parameters. All high-confidence mutations were identified using our in-house pipeline coupled with visual inspection and then annotated with ANNOVAR (version: 2016Feb01).

Copy number alteration analysis

Copy number alterations (CNAs) were detected in the WES data by CONTRA.[3] CNAs with a copy ratio of ≥1.25 were classified as amplification, and those with a copy ratio of ≤0.75 were classified as a deletion.

Amino acid sequence alignment of *SETD1B* across multiple species

The amino acid sequences of the *SETD1B* protein from *Homo sapiens*, *Mus musculus*, *Gallus gallus* and *Xenopustropicalis* were retrieved from Ensembl and aligned using ClustalW in the DNASTAR Lasergene software suite.

Computational modeling of *SETD1B* and validation of the model

The automated server program I-TASSER was employed with its default parameters to build the model according to the homology modeling method.[4,5] The stereochemical quality of the models was verified with the program PROCHECK to select the best model.[6] The 3D profile of the residue was generated by the Verify3D Structure Evaluation Server and QMEAN.[7,8] The model was created using PyMOL (www.pymol.org).

Cell culture

The human embryonic kidney cell line HEK293T (American Type Culture Collection) was maintained in DMEM GlutaMAX (Life Technologies, Carlsbad, CA) supplemented with 10% fetal bovine serum and penicillin/streptomycin (Life Technologies) and incubated at 37°C in an environment containing 5% CO_2. We authenticated the source of the cell lines

and tested for mycoplasma contamination; we did not observe cross-contaminated cell lines or mycoplasma contamination.

Plasmid construction

To construct the *SETD1B* wild-type plasmid, we cloned the *SETD1B* ultimate open reading frame (ORF) clone into a *pCDF* vector under the control of an *hCMV* promoter. The three *SETD1B* mutations (S487L, C931Y and A1054del) were generated by PCR mutagenesis using the Q5 Site-Directed Mutagenesis Kit (New England Biolabs, Ipswich, MA) on the *pCDF-SETD1B* plasmid according to the manufacturer's instructions.

Immunohistochemistry

Paraffin-embedded tumor sections were deparaffinized using standard protocols. The sections were blocked in 10% goat serum in phosphate-buffered saline (PBS) containing 0.5% Triton X-100 for 30 min, incubated with an anti-*SETD1B* antibody (Abcam, Cambridge, UK, Cat. No: ab113984) and detected using the HRP Rabbit DAB Detection System. Images were acquired at 400× magnification and processed using an Olympus microscope system. The mitotic index of the tumors was recorded as the number of mitotic figures in 10 high-power fields.

Cell growth and colony formation assays

Anchorage-dependent cell growth was evaluated using a CCK-8 Kit (Dojindo Laboratories, Kumamoto, Japan) according to the manufacturer's protocols. For the colony formation assay, transfected cells were cultured in six-well plates for 2 weeks, after which the colonies were fixed with 4% paraformaldehyde and stained with crystal violet for 30 min. The number of colonies with a diameter greater than 1.5 mm was counted.

Cell cycle analysis

Cell cycle analysis was conducted using flow cytometry as described previously.[9,10] Briefly, cells were fixed in 70% ethanol for at least 18 hr, washed with PBS, and incubated with RNase A (0.2 mg/ml) in PBS. Propidium iodide was then added to the cell suspension, and the samples were analyzed on a FACS Calibur flow cytometer (Becton Dickinson, Franklin Lakes, NJ).

Apoptosis and flow cytometry analysis

An AnnexinV assay (BD) was performed according to the manufacturer's protocols to assess apoptosis. Briefly, cells were harvested after transfection with either the wild-type or mutant *SETD1B* plasmids, washed twice with PBS, incubated with FITC-conjugated AnnexinV for 15 min, and measured by flow cytometry (FCM) using the FACScan flow cytometer (BD).

Cell migration and invasion assays

Wound healing assays were used to assess cell migration. Briefly, transfected cells were cultured in six-well plates until they formed confluent monolayers; the cell layer was then mechanically scratched using a 1-ml pipette tip to create a wound. The cells were washed

with PBS to remove cellular debris and cultured for an additional 24 hr to permit wound healing. Cell invasion was determined by seeding cells into the upper chamber of a Transwell plate (Corning, NY) coated with Matrigel (BD Biosciences, San Jose, CA). After 18 hr, cells that had invaded through the Matrigel membrane were fixed with 4% paraformaldehyde and stained with crystal violet. The number of invading cells was counted in five randomly selected microscopic fields, and the fields were photographed.

Statistical analysis

Statistical analysis was performed with either the SPSS Version 20.0 statistical software package or GraphPad Prism 6 software. Continuous variables were analyzed using either Student's *t*-test or the Mann–Whitney test. Categorical data were compared using either Fisher's exact test or the χ^2 test. Overall survival (OS) was defined from the date of diagnosis to the date of death or to the date of the last follow-up. A value of $p \leq 0.05$ was considered to indicate statistical significance.

Data availability

The raw sequencing data from our study have been deposited in the Genome Sequence Archive of the Beijing Institute of Genomics at the Chinese Academy of Sciences (http://gsa.big.as.cn/) with the accession number PRJCA000559. Data that support the findings of our study are available from The Cancer Genome Atlas (TCGA) database (http://cancergenome.nih.gov).

Results

Mutational landscape

To explore the molecular pathogenesis of PHNETs and gain a better understanding of the complete landscape of somatic mutations in PHNETs, we first performed WES of DNA from paired tumor/normal tissues from 22 PHNET patients. A summary of the clinical and demographic information of the patients included in the tumor cohort is provided in Supporting Information Table S1. The average sequencing depth was approximately 181-fold (145X–234X) and 98.0% (96.9–98.6%) of the target regions were covered at least 10-fold (Supporting Information Fig. S1a and S1b, Supporting Information Table S2). We identified a total of 777 somatic mutations involving 726 genes, including 194 synonymous, 419 missense, 37 nonsense, 7 splice-site and 120 insertion or deletion (indel) mutations, with a median of 1.07 mutations per megabase (Mb; range 0.15–4.42) in 22 PHNET patients (Supporting Information Tables S3 and S4). Then, we performed GO-Term and Pathway enrichment analysis of these mutant genes, *p* values were defined by the DAVID algorithm. The enriched GO terms included nuclear chromatin, protein phosphorylation and ATP binding, and so on (Supporting Information Table S5). The results of the KEGG enrichment analysis showed that mutant genes mainly enriched in central carbon metabolism in cancer and FoxO signaling pathway (Supporting Information Table S6). Among those mutations, *SETD1B* and *TP53* represented the most frequently mutated genes (3/22 subjects for both genes, 13.6%; Supporting Information Table S7). We analyzed the somatic mutations of prominent genes using the MutSigCV method and found that none of them were significantly mutated genes with $q < 0.1$ (Supporting Information Table S8). The most

common substitution among these samples was the C:G>T:A mutation, which is similar to the substitution patterns reported in most cancer types[11] (Supporting Information Fig. S2 and Table S9). The somatic nonsilent mutation load per individual varied remarkably and did not significantly correlated with the clinical stage of the disease, the hepatitis B virus (HBV) infection status, or the subject's age. A high somatic mutation burden (≥1.5/Mb) was associated with poor prognosis in PHNET patients ($p < 0.001$, log-rank test; Supporting Information Fig. S3). Intriguingly, G3 grade tumors exhibited the highest percentage of mutations. A significant increase in tumor grade G3 was associated with the number of somatic mutations and correlated with a more aggressive phenotype.

In the data from 22 patients with PHNETs, we performed a somatic CNA analysis and identified acquired genomic alterations that showed considerable variability across the individual tumors. Among the minimal common regions, amplifications in chromosomes 5p, 17p, 17q, 19p, 19q, 20p and 20q as well as copy number deletions in chromosomes 1p, 10q, 11q and 13q were most frequently observed (Supporting Information Fig. S4 and Table S10). Furthermore, we observed the deletion of *CDKN2C*, *NRAS*, *TLX1*, *RHOC*, *RUNX3* and *E2F2* and the amplification of *ERBB2*, *GNA11*, *MAFB* and *TCF3*, suggesting that alterations in the expression of these genes might be a common event related to PHNETs.

SETD1B mutations in PHNETs

We sought to clarify the pathogenic roles of genes and better define their mutation prevalence among individuals with PHNETs. In total, 22 recurring mutated genes were identified; of these, *TP53* and *SETD1B* were the most frequently mutated genes among the 22 PHNET patients (Fig. 1). Somatic mutations in *TP53* (E214X, E154K and 83del) were identified in three out of the 22 samples and were mainly located in the functional domain of *p53*. Notably, the frequency of *TP53* mutations among PHNET patients was much lower than that among hepatocellular carcinoma (HCC) and intrahepatic bile duct carcinoma patients.[12–14] Interestingly, these mutations were associated with poor prognosis in PHNET patients ($p < 0.001$, log-rank test; Supporting Information Fig. S5).

The multiple endocrine neoplasia type 1 (*MEN1*) gene encodes menin, a putative tumor suppressor associated with multiple endocrine neoplasia type 1. Previous studies have shown that *MEN1* is an important molecule in NETs that is frequently mutated in pancreatic neuroendocrine, parathyroid and pituitary tumors.[15,16] In two out of 22 PHNET patients, we identified two novel *MEN* mutations (R420X and 128del) in loci that are distinct from previously identified loci of *MEN1* gene mutations; these two novel mutations were located in the menin domain (Supporting Information Fig. S6), suggesting that they may be related to PHNET pathogenicity.

SETD1B, a SET domain containing 1B gene, is a component of the histone methyltransferase complex that produces trimethylated histone H3 at Lys4 and has been implicated in multiple biological processes.[17] Given that we identified *SETD1B* gene abnormalities as the most frequent somatic mutations in PHNET patients, we hypothesized that this gene plays an essential role in the pathogenesis of PHNETs. Three *SETD1B* somatic mutations (S487 L, C931Y and A1054del) were identified in three out of the 22 patient samples (Supporting Information Fig. S7). It is interesting that these mutations are

not located in the domain regions (Fig. 2a); however, when we assessed the evolutionary conservation of two single-nucleotide variations (SNVs) and one nonframe shift deletion of *SETD1B*, we found that these mutations are located in domains in which amino acid sequences are highly conserved across species (Fig. 2b). Next, we investigated the effects that these mutations might exert on the structure of *SETD1B* and found that the predicted mutant *SETD1B* structure exhibits great changes; thus, a *SETD1B* model was constructed and validated using the homology modeling method and the I-TASSER server. We speculated that the *SETD1B* mutations are closely related to the orientation of the C-terminal domain of the protein and that these mutations most likely alter protein function. Changes in the C-terminal orientation of *SETD1B* may affect its interaction with other proteins (Fig. 2c). In addition, we found that *SETD1B* had a mutation rate greater than 5% in colon adenocarcinoma, malignant lymphoma, ovarian cancer and endocrine pancreatic cancer using the International Cancer Genome Consortium (ICGC) database (Fig. 2d). To explore the clinical significance of *SETD1B* mutations, the patients in the cohort were divided into wild-type and mutant subgroups. Our analysis showed that subjects with *SETD1B* mutations had a worse prognosis than subjects without mutations in this gene (p = 0.046, log-rank test) as reflected by OS (Fig. 2e). To verify this association, we analyzed 8,872 samples from TCGA database with complete survival information and found that the association between *SETD1B* mutations and prognosis was also significant ($p < 0.001$, log-rank test; Fig. 2f). The clinical information of 56 “Mut SETD1B” cases in TCGA was shown (Supporting Information Table S11). We also observed that there were significant differences in overall mutation burden between the “Mut SETD1B” and the “WT SETD1B” in TCGA cases (Supporting Information Fig. S8). In addition, *SETD1B* mutations may correlate with tumor grade in PHNET patients (Supporting Information Fig. S9). Taken together, the correlation of *SETD1B* mutations with advanced disease stage and poor clinical outcome might explain the aggressive behavior of PHNETs with mutated *SETD1B*.

Functional analysis of *SETD1B* alterations

To gain further insight into the role of *SETD1B* mutations in PHNETs, we evaluated *SETD1B* levels by immunohistochemistry in formalin-fixed, paraffin-embedded PHNET samples. PHNET tissues that expressed wild-type (WT) *SETD1B* showed robust staining for *SETD1B*, whereas tumor cells from PHNETs with the *SETD1B* A1054del mutation showed significantly decreased *SETD1B* expression (Fig. 3a). However, tumors with the *SETD1B* S487L and C931Y mutations did not exhibit obvious differences in *SETD1B* expression compared to tumors that express WT *SETD1B* protein. Similarly, the *SETD1B* expression levels of paired adjacent tissues in the mutant group (S487L and C931Y) were similar to those of paired adjacent tissues in the WT *SETD1B* group (Supporting Information Fig. S10). Immunohistochemical staining of *SETD1B* in the tumors and in paired adjacent noncancerous hepatic tissues was compared to that in HCC tissues as a control (Supporting Information Fig. S11). To explore the functional consequences of the identified *SETD1B* mutations, we constructed vectors expressing either wild-type or mutant *SETD1B* protein (S487L, C931Y or A1054del) and transiently transfected HEK293T cells with these vectors. All primer sequences are provided in Supporting Information Table S12. By observing the anchorage-dependent growth of HEK293T cells, we found that HEK293T cells transfected with the *SETD1B* A1054del mutant grew much faster than cells transfected with either the

SETD1B S487L or C931Y mutant or cells expressing wild-type *SETD1B* (Fig. 3b). To elucidate the mechanism through which *SETD1B* promotes cell growth, we investigated the effects of *SETD1B* on the cell cycle using flow cytometry. Compared to HEK293T cells expressing wild-type *SETD1B*, the percentage of HEK293T cells expressing the *SETD1B* A1054del mutant in G0/G1 phase (from 51.51% to 42.03%) and G2/M phase (from 36.13% to 21.72%) was remarkably reduced, whereas the percentage of HEK293T cells expressing the *SETD1B* A1054del mutant in S phase was increased (from 12.36% to 36.25%). In contrast, neither the S487L nor the C931Y mutation in *SETD1B* significantly changed the percentage of cells in G0/G1, G2/M or S phase (Fig. 3c). Moreover, colony formation assays revealed that the colony number and colony size were larger in cells transfected with the *SETD1B* A1054del mutant than in cells expressing the *SETD1B* S487L or C931Y mutations or wild-type *SETD1B* (Fig. 3d). In addition, the three *SETD1B* mutants did not appear to regulate apoptosis compared to wild-type *SETD1B* (Supporting Information Fig. S12).

To determine the effects of the *SETD1B* mutations on cell migration and invasion, wound healing and Transwell invasion assays were performed. The wound healing assay demonstrated that the *SETD1B* A1054del mutation increased cell migration, but marked changes in motility were not observed in cells transfected with either the *SETD1B* S487L or C931Y mutant compared to cells expressing wild-type *SETD1B* (Fig. 3e). Similarly, the Transwell invasion assay revealed that the *SETD1B* A1054del mutation significantly enhanced the number of invading cells, whereas no differences in the number of invading cells were observed among cells expressing the *SETD1B* S487L or C931Y mutant compared to those expressing wild-type *SETD1B* (Fig. 3f). These data suggest that the *SETD1B* deletion mutation contributes to the tumorigenesis of PHNETs by promoting cell proliferation, migration and invasion and that it may be a potential prognostic marker and/or a therapeutic target for PHNETs.

Dysregulated pathways in PHNETs

We analyzed all of the nonsilent mutations from the 22 PHNET patients and identified genomic alterations that were relevant to several important processes, including epigenetic modifications, the cell cycle and neural development. The changes we observed indicate that abnormalities in these processes might be involved in PHNET tumorigenesis (Fig. 4). Interestingly, we found that epigenetic modifications in the tumor cells were mostly associated with the activity of H3K4 methyltransferases (*HMTs*), including *SETD1B* and *WDR5*; nucleosome remodeling factors (*NURF*), including *BPTF*, *RBBP4* and *HIST1H3A*; and histone deacetylase complexes (*HDACs*), including *HDAC1*. *MEN1* acts as a corepressor of *JunD* transcriptional activity via *HDAC* recruitment.[18] *HDAC1* has been coprecipitated with *WDR5*, which has been shown to directly regulate histone methylation and recruit *HDACs* to histone-bound DNA. Genetic alterations of the cell cycle in PHNETs primarily manifest as distinct defects in the G1/S transition, as demonstrated by the presence of *TP53* mutations in three out of 22 cases, *ATM*, *ATAD5*, *MED12* and *DIDO1* mutations in two cases, and *PTEN* and *BRD4* mutations in one case. Neural development is another process in which the mutated genes in PHNETs, including *UBR4*, *MEN1*, *GLUL*, *MECP2* and *GIGYF2*, displayed prominent enrichment. Mutations associated with these three

processes were observed in 12 out of the 22 PHNET cases (Supporting Information Table S13). Altogether, these results highlight the potential cooperative roles of these processes in PHNET pathogenesis.

In an effort to identify therapeutic targets for PHNETs, we correlated the identified genomic mutations with novel targeted therapeutic approaches that have been approved for clinical use or are currently undergoing clinical trials. In this manner, we identified 13 mutated genes that can potentially be targeted for the treatment of PHNETs[19] (Supporting Information Tables S14 and S15). These genes and their products represent druggable candidate targets and warrant further investigation.

Discussion

To the best of our knowledge, this is the first study in which WES was used to identify somatic alterations in PHNETs. In this report, we analyzed 22 PHNET patients and categorized 22 recurring mutated genes, including *TP53*, *SETD1B* and *MEN1*. Among these genes, *SETD1B* and *TP53* were shown to have the highest frequency of recurring mutations. Of note, the association between *SETD1B* and PHNETs is a novel finding. Additional immunohistochemical and biological analyses suggested the functional relevance of *SETD1B* in PHNETs. More importantly, we determined that multiple genes involved in epigenetic modification, the cell cycle and neural development are dysregulated in PHNETs.

MEN1 encodes the histone modifier menin, and its inactivation drives various phenotypes, including widespread transcriptional dysregulation via histone modification. *In vitro* studies have shown that menin localizes to the nucleus, possesses two functional nuclear localization signals and inhibits *JunD*-associated transcriptional activation. Most genomic alterations of *MEN1* affect one or all of the domains of menin that interact with *JunD*, *Smad3* and *NF-κB*, three major effectors of transcription and cell growth regulation.[20] A previous study identified several germline mutations in the *MEN1* gene among Japanese *MEN1* families[21] and among patients with glucagonoma and obesity.[22] Moreover, inactivation of *SETD1B*, which has a broad range of functions, directly influences these three key processes: epigenetic modification, cell cycle and neural development (Fig. 4). *SETD1B*, encoding a histone 3 lysine 4 methyltransferase, is a component of the *SET1* complex (*SET1C*)/COMPASS complex that participates in many life processes, such as the oncogenic gene expression program and Spemann's organizer gene activation in Xenopus.[17] *SETD1B* is a maternal effect gene required for the oogenic gene expression program[23] and a novel recurrently mutated gene in chronic myeloid leukemia.[24] *SETD1B* is essential for hematopoietic stem and progenitor cell homeostasis in adult mice.[25] *De novo* variants in *SETD1B* are associated with intellectual disability, epilepsy and autism.[26] Tang Z's group reported robust *SET1C*-mediated H3K4 trimethylation that is dependent upon p53- and p300-mediated H3 acetylation. They also established a mechanism by which *SET1C* and p300 act cooperatively, through direct interactions and coupled histone modifications, to facilitate the function of p53.[27] Previous studies have shown that *SETD1B* associates with a 450-kDa complex that contains all five noncatalytic components of the SET1A complex: *CFP1*, *Rbbp5*, *Ash2*, *WDR5* and *Wdr82*.[28] Concomitant *SET1A* and *SETD1B* localization appears as largely nonoverlapping puncta along the euchromatin in the nucleus, suggesting

that each protein binds to a unique set of target genes, thereby making non-redundant contributions to the epigenetic control of chromatin structure and gene expression.[29,30] The mixed lineage leukemia (*MLL*) family of proteins (including *MLL1-MLL4*, *SET1A* and *SETD1B*) specifically methylatesLys4 of histone H3 and plays a pivotal role in the transcriptional regulation of genes involved in hematopoiesis and development.[31,32] Recent studies have provided evidence that *TP53* is the target of *SET1/COMPASS* and have suggested that these genes may cooperate and function as a tumor suppressor.[27,28] Furthermore, the acetylation-regulated interaction between *p53* and *SET* is part of a widespread regulatory process.[33] Li *et al.* revealed a synergistic role of hSET1 and NURF in regulating the USF-bound barrier insulator that prevents erythroid genes from encroaching upon heterochromatin.[34] Chromatin remodeling related genes (*KMT2D*, *KMT2C*, *SETD1B* and *BCOR*) is frequently mutated in endometrioid endometrial carcinoma.[35] Collectively, we concluded that gene-oriented (*SETD1B*) and pathway-oriented networks are dependent and cooperative and require further investigation in PHNETs. In addition, the main downstream target of *SETD1B* and how this *SETD1B* mutation regulates its function warrant to be elucidated in subsequent studies.

NETs are a rare type of malignancy. Understanding the molecular basis of PHNETs at the genome level will be very important for therapeutic development. This report represents the first and largest genome-wide DNA sequencing study of PHNETs ever performed. However, given the number of tumors and normal tissue pairs, we analyzed and the observed mutational frequency in PHNETs, our study had sufficient power to identify only genes with high-frequency mutations (i.e., >10%). Interestingly, the *SETD1B* mutations were present in all G3 stage tumor samples, in which the mutation burden is highest, and we also found that individuals with *SETD1B* mutations in TCGA had a much worse prognosis. Due to the high prognostic relevance of the mutation rate and the cooccurrence of two out of three SETD1B mutations with this increased mutation burden, whether SETD1B missense mutations are only passengers needs to be validated in much more PHNETs cohorts. Currently, there are no cell lines with which to perform functional work on this subtype of NETs, and the functional studies undertaken using HEK293T cells are limited in that HEK293T cells are not a primary liver NET cell line. However, a PHNET cell line is a high challenge question and remains to be investigated in a suitable experimental setting. Herein, our data showed that the novel *SETD1B* A1054del mutation promoted cell proliferation, migration and invasion compared to the wild-type protein. The functional analysis presented in this article seems to support a functional relevance of the A1054del mutations, while the two missense mutations only display no or insignificant effects. The likely reason is A1054del site is close to C-terminal which has complete opposite orientation in “Mut *SETD1B*” and “*WT SETD1B*” (Fig. 2c). Importantly, we analyzed the clinical characters of PHNETs with A1054del mutation. Despite the inframe indel A1054del appears in a sparsely mutated sample, this patient had shorter OS time than other patients with two missense mutations. To this end, we concluded that the somatic *SETD1B* mutation encoding A1054del is likely an activating mutation that contributes to PHNET tumorigenesis. Hence, additional studies should be performed to provide further insight into the biology of PHNETs and other somatic alterations involved in the tumorigenesis and malignant transformation of PHNETs. In addition to the fact that the low incidence of PHNETs has made it difficult to identify

statistically significant associations between specific mutations and the disease, many cases of PHNETs have clinically aggressive features, which suggests that interactions between somatic changes and prognosis in this and other rare cancers require further investigation. Of course, since PHNETs may arise from different tissues and tumor stages, it is necessary to consider the heterogeneous features of these tumors and the overall incidence of mutations. In addition to the identification of a specific mutation in *SETD1B*, our analysis identified many other potential diagnostic and therapeutic approaches for patients with PHNETs, which will offer additional opportunities to identify and treat this typically rare tumor.

Supplementary Material

Refer to Web version on PubMed Central for supplementary material.

Acknowledgements

We are grateful to Prof. Qimin Zhan (Peking University) for insightful discussions and helpful comments on the article. We acknowledge the International Cancer Genome Consortium (ICGC) and The Cancer Genome Atlas (TCGA) for sharing data.

Grant sponsor: Beijing Nova Program; **Grant number:** Z141107001814054; **Grant sponsor:** National Institute of Health Grant; **Grant number:** R01AI121180; **Grant sponsor:** National Natural Science Foundation of China; **Grant numbers:** 31570875, 31770948, 81771700; **Grant sponsor:** National High Technology Research and Development Program of China; **Grant numbers:** 2013ZX10004003, 2015AA020924

Abbreviations

CNAs	copy number alterations
FFPE	formalin-fixed paraffin-embedded
GI	gastrointestinal
NET	neuroendocrine tumors
OS	overall survival
PHNETs	primary hepatic neuroendocrine tumors
SETD1B	SET domain containing 1B gene
SNVs	single-nucleotide variations
WES	whole-exome sequencing

References

1. Caplin ME, Pavel M, Ruszniewski P. Lanreotide in metastatic enteropancreatic neuroendocrine tumors. N Engl J Med 2014;371:1556–7.
2. Rasmussen JO, von Holstein SL, Prause JU, et al. Genetic analysis of an orbital metastasis from a primary hepatic neuroendocrine carcinoma. Oncol Rep 2014;32:1447–50. [PubMed: 25051214]
3. Li J, Lupat R, Amarasinghe KC, et al. CONTRA: copy number analysis for targeted resequencing. Bioinformatics 2012;28:1307–13. [PubMed: 22474122]
4. Roy A, Kucukural A, Zhang Y. I-TASSER: a unified platform for automated protein structure and function prediction. Nat Protoc 2010;5:725–38. [PubMed: 20360767]

5. Zhang Y I-TASSER: fully automated protein structure prediction in CASP8. Proteins 2009;77: 100–13. [PubMed: 19768687]
6. Laskowski RA, Rullmannn JA, MacArthur MW, et al. AQUA and PROCHECK-NMR: programs for checking the quality of protein structures solved by NMR. J Biomol NMR 1996;8:477–86. [PubMed: 9008363]
7. Luthy R, Bowie JU, Eisenberg D. Assessment of protein models with three-dimensional profiles. Nature 1992;356:83–5. [PubMed: 1538787]
8. Bowie JU, Luthy R, Eisenberg D. A method to identify protein sequences that fold into a known three-dimensional structure. Science 1991;253: 164–70. [PubMed: 1853201]
9. Feng Y, Xu X, Zhang Y, et al. HPIP is upregulated in colorectal cancer and regulates colorectal cancer cell proliferation, apoptosis and invasion. Sci Rep 2015;5:9429. [PubMed: 25800793]
10. Song Y, Li L, Ou Y, et al. Identification of genomic alterations in oesophageal squamous cell cancer. Nature 2014;509:91–5. [PubMed: 24670651]
11. Ahmad J, Eng FJ, Branch AD. HCV and HCC: clinical update and a review of HCC-associated viral mutations in the core gene. Semin Liver Dis 2011;31:347–55. [PubMed: 22189975]
12. Lee JS. The mutational landscape of hepatocellular carcinoma. Clin Mol Hepatol 2015;21:220–9. [PubMed: 26523267]
13. Totoki Y, Tatsuno K, Covington KR, et al. Trans-ancestry mutational landscape of hepatocellular carcinoma genomes. Nat Genet 2014;46:1267–73. [PubMed: 25362482]
14. Llovet JM, Zucman-Rossi J, Pikarsky E, et al. Hepatocellular carcinoma. Nat Rev Dis Primers 2016;2:16018. [PubMed: 27158749]
15. Cao Y, Gao Z, Li L, et al. Whole exome sequencing of insulinoma reveals recurrent T372R mutations in YY1. Nat Commun 2013;4:2810. [PubMed: 24326773]
16. Jiao Y, Shi C, Edil BH, et al. DAXX/ATRX, MEN1, and mTOR pathway genes are frequently altered in pancreatic neuroendocrine tumors. Science 2011;331:1199–203. [PubMed: 21252315]
17. Lee JH, Tate CM, You JS, et al. Identification and characterization of the human Set1B histone H3-Lys4 methyltransferase complex. J Biol Chem 2007;282:13419–28. [PubMed: 17355966]
18. Hein MY, Hubner NC, Poser I, et al. A human interactome in three quantitative dimensions organized by stoichiometries and abundances. Cell 2015;163:712–23. [PubMed: 26496610]
19. Garnett MJ, Edelman EJ, Heidorn SJ, et al. Systematic identification of genomic markers of drug sensitivity in cancer cells. Nature 2012;483:570–5. [PubMed: 22460902]
20. Wautot V, Vercherat C, Lespinasse J, et al. Germline mutation profile of MEN1 in multiple endocrine neoplasia type 1: search for correlation between phenotype and the functional domains of the MEN1 protein. Hum Mutat 2002;20:35–47. [PubMed: 12112656]
21. Sato M, Matsubara S, Miyauchi A, et al. Identification of five novel germline mutations of the MEN1 gene in Japanese multiple endocrine neoplasia type 1 (MEN1) families. J Med Genet 1998; 35:915–9. [PubMed: 9832038]
22. Murakami T, Usui T, Nakajima A, et al. A novel missense mutation of the MEN1 gene in a patient with multiple endocrine neoplasia type 1 with glucagonoma and obesity. Intern Med 2015;54: 2475–81. [PubMed: 26424307]
23. Brici D, Zhang Q, Reinhardt S, et al. Setd1b, encoding a histone 3 lysine 4 methyltransferase, is a maternal effect gene required for the oogenic gene expression program. Development 2017;144: 2606–17. [PubMed: 28619824]
24. Branford S, Wang P, Yeung DT, et al. Integrative genomic analysis reveals cancer-associated mutations at diagnosis of CML in patients with high-risk disease. Blood 2018;132:948–61. [PubMed: 29967129]
25. Schmidt K, Zhang Q, Tasdogan A, et al. The H3K4 methyltransferase Setd1b is essential for hematopoietic stem and progenitor cell homeostasis in mice. Elife 2018;7:e27157. [PubMed: 29916805]
26. Hiraide T, Nakashima M, Yamoto K, et al. De novo variants in SETD1B are associated with intellectual disability, epilepsy and autism. Hum Genet 2018;137:95–104. [PubMed: 29322246]
27. Tang Z, Chen WY, Shimada M, et al. SET1 and p300 act synergistically, through coupled histone modifications, in transcriptional activation by p53. Cell 2013;154:297–310. [PubMed: 23870121]

28. Duncan EM, Chitsazan AD, Seidel CW, et al. Set1 and MLL1/2 target distinct sets of functionally different genomic loci in vivo. Cell Rep 2015;13:2741–55. [PubMed: 26711341]
29. Calo E, Wysocka J. Modification of enhancer chromatin: what, how, and why? Mol Cell 2013; 49:825–37. [PubMed: 23473601]
30. Putiri EL, Tiedemann RL, Liu C, et al. Impact of human MLL/COMPASS and polycomb complexes on the DNA methylome. Oncotarget 2014;5:6338–52. [PubMed: 25071008]
31. Li Y, Han J, Zhang Y, et al. Structural basis for activity regulation of MLL family methyltransferases. Nature 2016;530:447–52. [PubMed: 26886794]
32. Yang W, Ernst P. Distinct functions of histone H3, lysine 4 methyltransferases in normal and malignant hematopoiesis. Curr Opin Hematol 2017;24:322–8. [PubMed: 28375985]
33. Wang D, Kon N, Lasso G, et al. Acetylation-regulated interaction between p53 and SET reveals a widespread regulatory mode. Nature 2016;538: 118–22. [PubMed: 27626385]
34. Li X, Wang S, Li Y, et al. Chromatin boundaries require functional collaboration between the hSET1 and NURF complexes. Blood 2011;118: 1386–94. [PubMed: 21653943]
35. Garcia-Sanz P, Trivino JC, Mota A, et al. Chromatin remodelling and DNA repair genes are frequently mutated in endometrioid endometrial carcinoma. Int J Cancer 2017;140:1551–63. [PubMed: 27997699]

What's new?

Neuroendocrine tumors often metastasize to the liver but primary hepatic neuroendocrine tumors are extremely rare. Here the authors sequenced tumors from 22 patients in China and provide a first look at the mutational landscape of primary hepatic neuroendocrine tumors. The study points to a possible etiological role of the SET domain containing 1B gene (SETD1B) as it was among the most frequently mutated genes, a role that needs to be further explored.

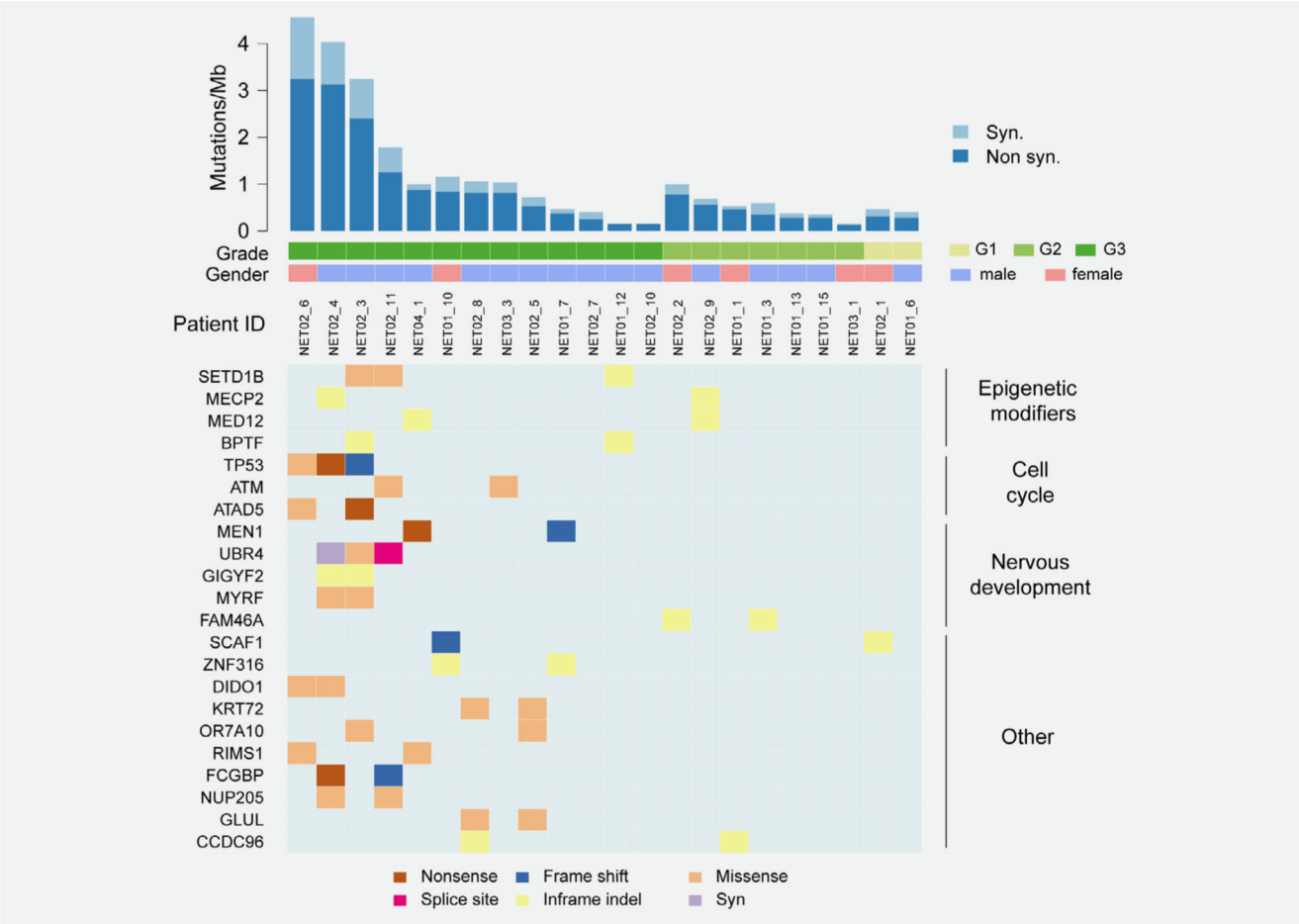

Figure 1.

Whole-exome sequencing and mutated genes in 22 patients with PHNETs. Each column represents an individual tumor, and each row denotes a single gene. The rates of somatic mutations in each examined tumor sample are expressed as the number of mutations per megabase (Mb) of the covered target sequence (top). Also shown are the key clinical parameters (middle) and the significantly mutated genes (SMG) colored by the type of mutation.

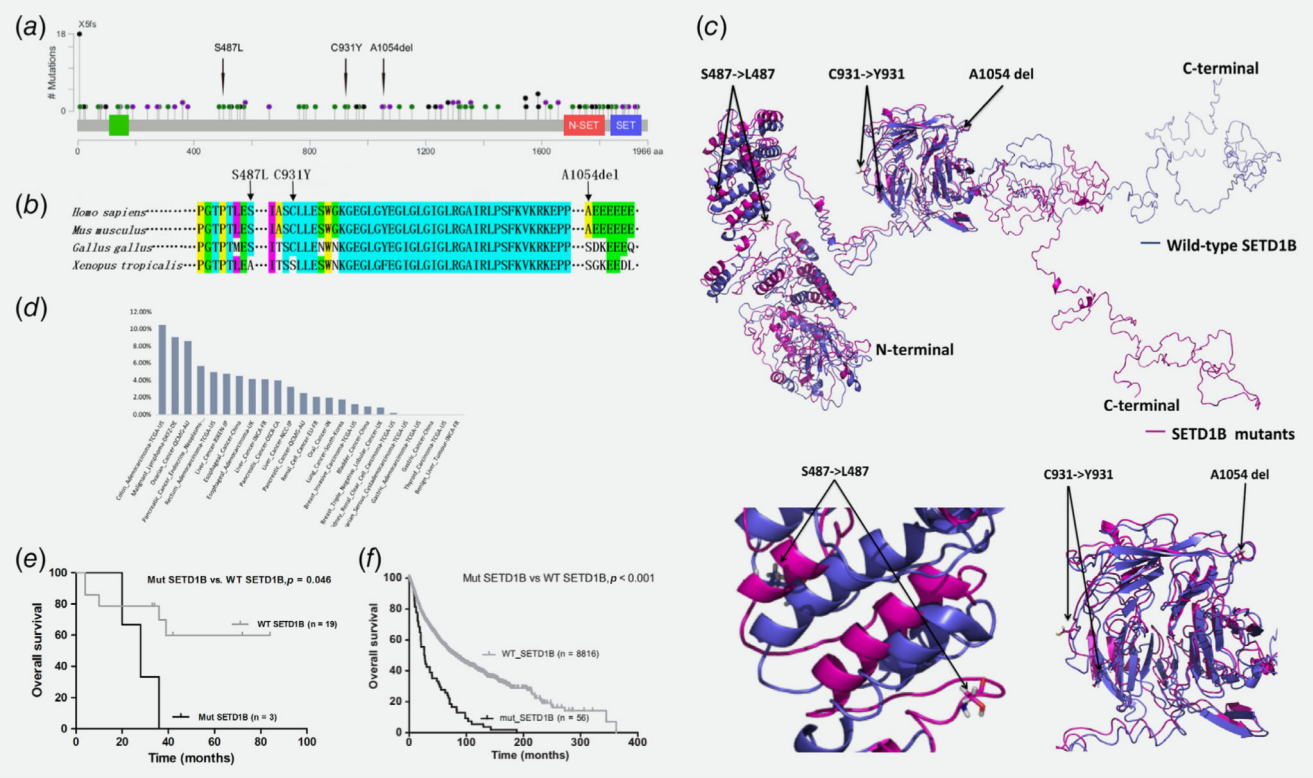

Figure 2.

SETD1B mutations in PHNETs. (*a*) Schematic representation of the domain structure and locations of the somatic mutations within *SETD1B* observed in our study and collected from the ICGC database. (*b*) Sequence alignment of the *SETD1B* protein across distinct species. (*c*) Prediction of the structures of the *SETD1B* mutants. (*d*) Frequency of samples from the ICGC database with *SETD1B* mutations. (*e*) Overall survival (OS) of patients with PHNETs according to the mutation status of *SETD1B* ($p = 0.046$, log-rank test). (*f*) Overall survival (OS) of patients in TCGA database according to the mutation status of *SETD1B* (***$p <$ 0.001, log-rank test). Survival analysis was conducted based on results of Broad Institute TCGA Genome Data Analysis Center (2015): Firehose stddata__2015_11_01 run. Broad Institute of MIT and Harvard. doi: 10.7908/C1571BB1. The mutation and clinic data were downloaded from the Broad TCGA GDAC site (http://gdac.broadinstitute.org/runs/stddata__2015_11_01/data/).

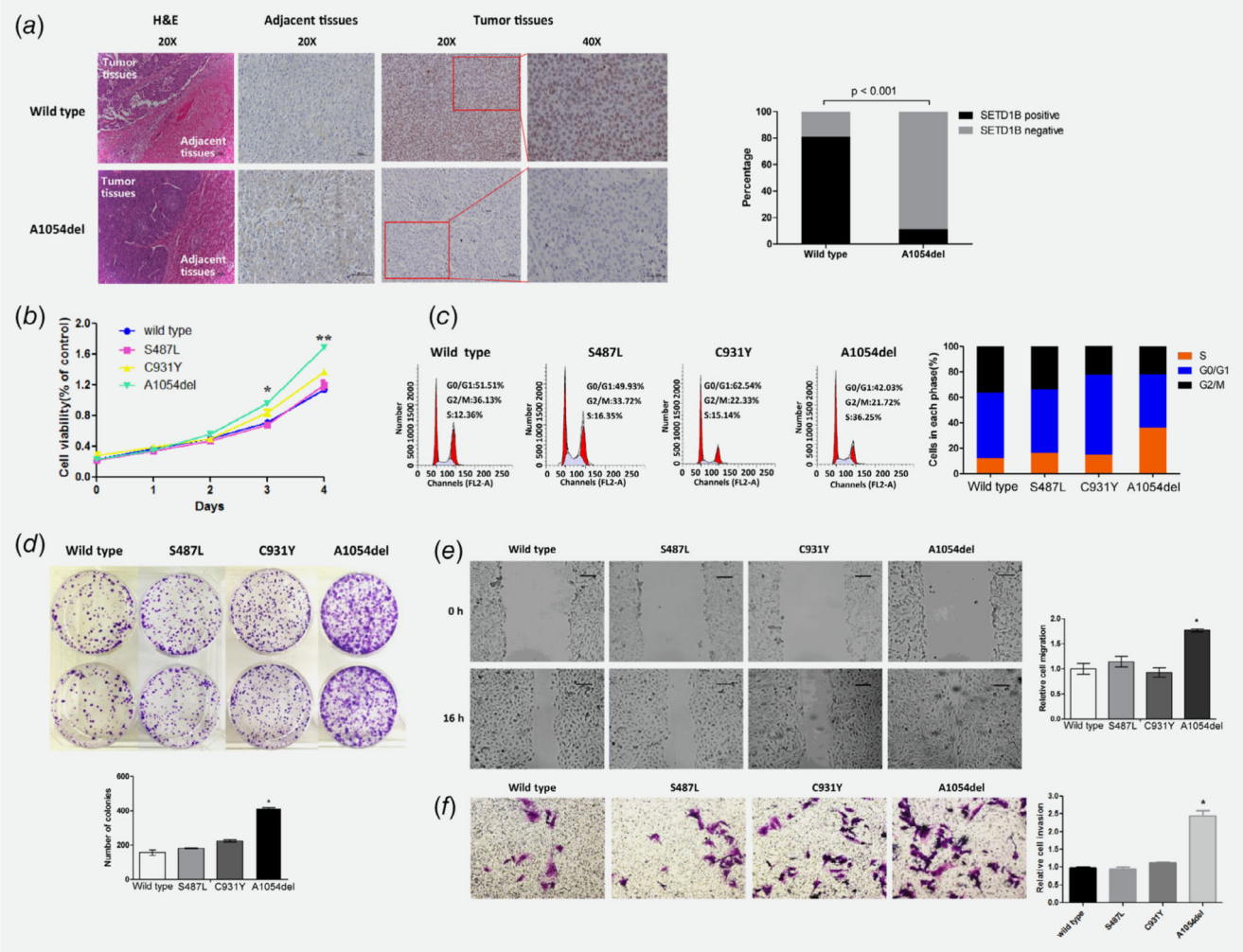

Figure 3.

Functional analysis of the *SETD1B* mutations. (*a*) Representative micrographs of *SETD1B* protein expression as assessed by immunohistochemistry in PHNET specimens expressing the A1054del mutant and wild-type *SETD1B* (***$p < 0.001$, *t*-test). Scale bars, 500 μm. (*b*) HEK293T cells transfected with either wild-type or mutant *SETD1B* (S487L, C931Y and A1054del) were grown in regular medium and harvested at the indicated times. The cell number was determined using CCK-8 assays when compared to WT *SETD1B* (*$p < 0.05$ and **$p < 0.01$, respectively, *t*-test). (*c*) Flow cytometry analysis of the cell cycle in HEK293T cells transfected with either wild-type or mutant *SETD1B* (S487L, C931Y and A1054del). (*d*) Colony formation assays using HEK293T cells transfected as described in *b*, when compared to WT *SETD1B* (***$p < 0.001$, *t*-test). All values are presented as the mean ± SD of triplicate measurements. (*e*) Migration of HEK293T cells transfected with wild-type or mutant*SETD1B* (S487L, C931Y and A1054del) was determined using the wound healing assay (**$p < 0.01$, *t*-test). The images shown here are representative of the three experimental replicates for each condition. (*f*) Cell invasion of HEK293T cells transfected with wild-type or mutant *SETD1B* (S487L, C931Y and A1054del) was assessed using a Matrigel-coated invasion chamber. Invading cells were fixed and stained with crystal violet

when compared to WT *SETD1B* (*$p < 0.05$, *t*-test). Scale bar: 100 μm. Error bars represent the standard deviation (SD) from at least three independent experiments.

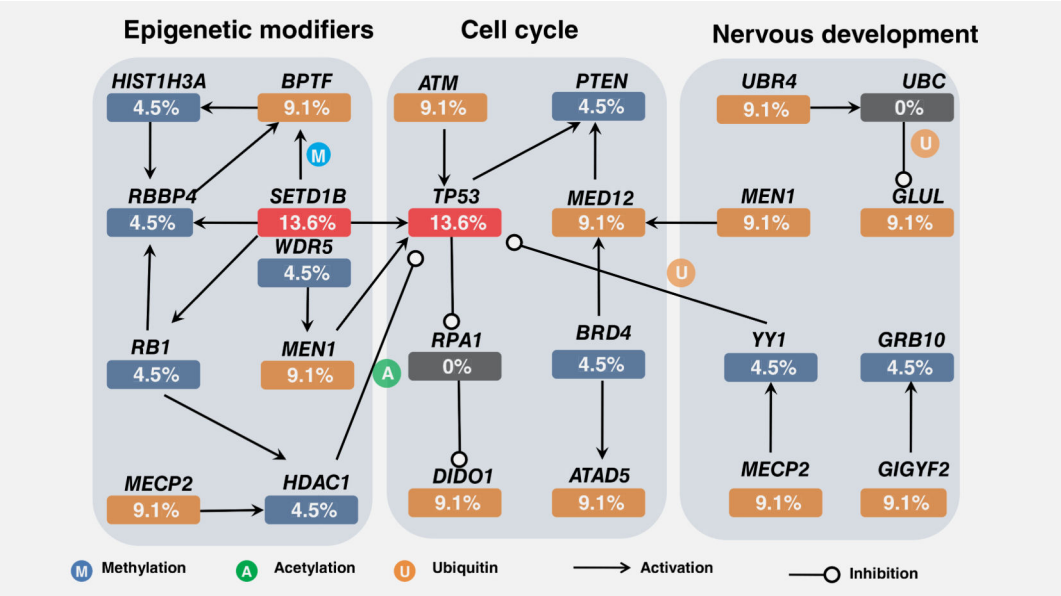

Figure 4.

Somatically altered pathways in PHNETs. Proteins associated with somatic mutations are affiliated with (from left to right) epigenetic modification, cell cycle or neural development. The frequencies of alterations are expressed as a percentage of all patient samples.